buildings

MDPI

Article

A Study on the Mechanical Properties and Microcosmic Mechanism of Basalt Fiber Modified Rubber Ceramsite Concrete

Changming Bu [1,2], Dongxu Zhu [1,2], Lei Liu [1,2], Xinyu Lu [1,2], Yi Sun [1,2,*], Zhitao Yan [1,2,*], Linwen Yu [3] and Qike Wei [4]

1 School of Civil Engineering and Architecture, Chongqing University of Science & Technology, Chongqing 401331, China; buchangming@cqust.edu.cn (C.B.); 2020206029@cqust.edu.cn (D.Z.); 2020206111@cqust.edu.cn (L.L.); 2020206077@cqust.edu.cn (X.L.)
2 Chongqing Key Laboratory of Energy Engineering Mechanics & Disaster Prevention and Mitigation, Chongqing 401331, China
3 School of Materials Science and Engineering, Chongqing University, Chongqing 400044, China; linwen.yu@cqu.edu.cn
4 China Metallurgical Construction Engineering Group Construction, Ltd., Chongqing 400084, China; weiqike@cmccltd.com
* Correspondence: sunyi@cqust.edu.cn (Y.S.); 2016023@cqust.edu.cn (Z.Y.); Tel.: +86-135-9416-9610 (Y.S.)

Abstract: In order to solve the problem of black pollution in the 21st century, a new type of rubber ceramsite concrete was prepared by pulverizing waste rubber tires into granules and adding aggregate to the ceramsite concrete. In order to reduce the weakening of mechanical properties of rubber, basalt fiber was used to modify the rubber. In this study, the compressive strength and splitting tensile strength of concrete specimens at days 3 and 28 were measured, the variation rule of compressive strength was explained based on the appearance of the microstructure, and the internal porosity of cubic specimens was characterized by the water absorption size. At the same time, an ultrasonic wave velocity test was used to test the uniformity and pore distribution of the block. The results showed that, with the increase in the rubber content, the compressive strength of rubber ceramsite concrete increases first and then decreases. The addition of basalt fiber can improve the compressive strength of the concrete. Water absorption is negatively correlated with compressive strength. Porosity is also negatively correlated with ultrasonic wave velocity. The basalt fiber length has no significant effect on the splitting tensile strength.

Keywords: ceramsite concrete; microscopic research; basalt fiber; compressive strength; rubber

Citation: Bu, C.; Zhu, D.; Liu, L.; Lu, X.; Sun, Y.; Yan, Z.; Yu, L.; Wei, Q. A Study on the Mechanical Properties and Microcosmic Mechanism of Basalt Fiber Modified Rubber Ceramsite Concrete. *Buildings* **2022**, *12*, 103. https://doi.org/10.3390/buildings12020103

Academic Editor: Tao Wang

Received: 31 December 2021
Accepted: 19 January 2022
Published: 21 January 2022

1. Introduction

Waste rubber products, such as used automobile tires, are traditionally unable to be properly recycled and treated, resulting in serious issues with black pollution. Exploring reasonable recycling and disposal methods is a primary task in order to solve this pollution problem [1,2]. Many scholars have conducted extensive studies on the incorporation of rubber into concrete, believing that it will significantly weaken the mechanical properties of concrete [3–11]. On this basis, the modification of rubber concrete has become an important research topic in this field; the most common modification methods are the modification of rubber aggregate and the addition of admixtures to rubber concrete [6,12]. There are two ways to study the modification of rubber aggregate: chemical and physical [13]. In the former, rubber aggregate is soaked in various chemical preparations, and the effect of the soaking treatment is optimized by water bath heating. Common chemical agents include NaOH [11,14,15], potassium permanganate [12,16], and hydrogen peroxide [17].

These chemical agents have the characteristics of high oxidation ability and strong alkalinity, which can greatly roughen the surface of rubber aggregate and allow it to more

closely combine with the cement matrix. Some scholars only use aqueous solutions for the soaking treatment [18]. Physical treatment is mainly conducted through microwave radiation [19–21], which is also aimed at roughening the rubber particles. A few studies have changed other properties of rubber particles through microwave radiation. Adding admixtures and fibers to rubber concrete is a widely used modification method. Commonly used admixtures include rubber latex [22,23], asphalt, and superplasticizer [23–25]. There are many kinds of fibers, and different fibers can be selected for modification research according to the specific application scenarios.

As the test matrix material, ceramsite concrete is a new lightweight concrete material mainly applied in the field of prefabricated building wall panels, with the main advantages of being lightweight, with good heat resistance and fire resistance [26]. Ceramsite concrete is mainly used in the bearing structure as a wall material to meet the basic strength requirement. Good plasticity and impact resistant ability are also important however, and these requirements can be realized through adding rubber aggregate and basalt fiber [3,27].

As a modified material, basalt fiber has comparable strength to steel fiber, a low production cost, high quality, and low price, giving it wide market application prospects [26]. There are few studies on basalt fiber in the academic research field, but the existing research results show that basalt fiber can significantly strengthen the connection between the aggregate inside the concrete, strengthen the interface transition zone of concrete, and improve various mechanical properties, including the compressive strength [17,28]. Choosing basalt fiber as a modified material is not only consistent with the movement towards green environmental protection but also helps to further explore the application prospects of this new fiber material.

In this study, 16 mesh rubber particles were used as the fine aggregate to replace river sand in traditional ceramsite concrete. The changes to the compressive strength and splitting tensile strength with three incorporation ratios were explored when mixing in basalt fibers, and the effects of basalt fibers of different lengths and dosages on the mechanical properties were compared. The mechanism was assessed using the water absorption, microscopic pattern, and ultrasonic wave velocity tests. The basic properties of ceramsite concrete and the characteristics of basalt fiber and rubber indicate that the research into the properties of new concrete materials combined with them is likely to be of social value and scientific significance.

2. Experimental Details

2.1. Test Raw Material

Cement was obtained from Chongqing Huanxin Yanjing Cement Co., Ltd. (Chongqing, China). The production of composite Portland cement P.C42.5R was in line with the national "General Portland cement" (GB175-2007) requirements.

The clay ceramsite was produced by Chongqing Caishan Ceramsite Factory (Chongqing, China), and its specific performance indicators are shown in Table 1.

Table 1. Performance parameters of ceramsite, rubber, and basalt fiber.

Ceramsite	**Particle Diameter**	**Density Grade**	**Bulk Density**	**Water Content**	**Apparent Density**	**Water Absorption**
	(mm)		(kg/m^3)	(%)	(kg/m^3)	(%)
	0–10	500	476	16.63	758.97	5.53
Rubber	**Particle Diameter**	**Mean Grain Size**	**Bulk Density**	**Ash Content**	**Apparent Density**	**Water Absorption**
	(mm)	(mm)	(kg/m^3)	(%)	(kg/m^3)	(%)
	1–3	1	1120	1<	1052	3<
Basalt Fiber	**Operating Temp**	**Sintering Temperature**	**Linear Density**	**Elastic Modulus**	**Density**	**Tensile Strength**
	(°C)	(°C)	(μm)	(GPa)	(kg/m^3)	(MPa)
	−269–650	1050	7–15	91–110	2630–2650	3000–4800

We used 10-mesh rubber granules produced by Chengdu Sitong Rubber and Plastic Co., Ltd. (Chengdu, China). See Table 1 for specific performance indicators.

The basalt fiber produced by Haining Anjie Material Co., Ltd. (Haining, China) was used, and its specific performance indicators are shown in Table 1.

2.2. Test Method

2.2.1. Compressive Strength

According to GB/T50081-2019, the samples used to assess compressive strength were cured for 3 and 28 days, respectively, in a constant temperature curing box at 20 ± 2 °C. The standard test method was used to measure the compressive strength. The sample size was 100 × 100 × 100 mm, with three pieces in each group and nine groups in total. The average value of the calculated results was taken [8,9].

$$f_c = \frac{F}{A} \quad (1)$$

where
f_c—Compressive strength of the sample (MPa);
F—Specimen failure load (N);
A—Specimen compression area (mm^2).

2.2.2. Splitting Tensile Strength

A 30T universal testing machine was selected, and a special fixture for measuring the splitting tensile strength was used for the corresponding tests [12,29]. According to GB/T50081-2019, the specimens were cured in a constant temperature curing box at 20 ± 2 °C for 28 d, and the splitting tensile strength standard test method was adopted for testing. The sample size was 100 × 100 × 100 mm, and each group had three pieces, with a total of nine groups. The results were averaged. Since a 100 × 100 × 100 cube specimen was selected for testing, referring to the specification, the final result was multiplied by a correlation coefficient of 0.85.

2.2.3. Microstructure

A Kyky-em 6200 scanning electron microscope (SEM) was used for the microstructure test. The object of observation was the debris in the central column of the specimen after crushing through the compressive strength test [9,30,31]. The selection of observation objects ensured that the fragments contained the necessary aggregates, such as rubber and ceramsite. At the same time, two kinds of aggregate rubber and ceramsite were studied separately. The post-treatment of the debris consisted of soaking in anhydrous ethanol for 24 h [3], which was intended to stop the hydration reaction of the concrete debris. The post-processing of the two aggregates was carried out through heat drying to ensure that the surface and interior of the aggregates were dry. During the test, the sample was soaked and drained of anhydrous ethanol on the surface, then was glued to the observation plate and placed in the gold-spraying instrument for gold-spraying treatment. The observation plate was sprayed several times until the surface was covered with a golden coating that could be observed by the naked eye. After that, the observation plate was placed in the sample chamber of the instrument for vacuumizing treatment, and finally, the observation and photography were carried out.

2.2.4. Water Absorption Test

Each group was set with three test blocks, for a total of 27 blocks. First, the test block was dried in a 105 °C drying box to a constant weight, denoted as M0. Then, it was immersed in water and removed every 24 h to dry the surface before testing its weight until it remained constant [32], denoted as M1. M1-M0 was taken as the water absorption quality, characterized by (M1 − M0)/(M0) = W, and W was the air content inside the generalized concrete specimen. The sample size was 100 × 100 × 100 mm.

2.2.5. Ultrasonic Wave Velocity Test

The Kh-500k ultrasonic wave velocity test method was selected, and each group consisted of three test blocks, for a total of 27 test blocks. Before the test, the test block was placed in a drying room for 48 h, and the ultrasonic wave velocity test was conducted after the excess water vapor was drained and preserved in the room [33]. The last three test values were averaged, and the three average values of each group were then averaged to obtain the ultrasonic wave velocity test value of each group. The sample size was 100 × 100 × 100 mm.

2.3. Test Proportions and Nomenclature

According to the applicable technical standard of lightweight aggregate concrete and the preliminary test, the optimal test ratio was selected for the following test, as shown in Table 2. Samples are numbered in the form of A-A-B-B-C-C, where A represents the content of basalt fiber, A is the specific value of the content of basalt fiber, B is the length of basalt fiber, B is the specific value of the length, C is the content of rubber, and C is the specific value of the content of the rubber. The result analysis simplified the grouping into the A-B-C form. Basalt fiber is an admixture, according to the volume percentage of direct incorporation. Rubber particles were replaced, and river sand was replaced proportionally with an equal volume.

Table 2. Mix proportion (kg/m^3).

ID \ Materials	Ceramsite	Cement	Water	Rubber	Fly Ash	Dosage	Length
A-0.2-B-9-C-10	774.64	369	150	18.5	81	0.2%	9
A-0.4-B-9-C-10	774.64	369	150	18.5	81	0.4%	9
A-0.6-B-9-C-10	774.64	369	150	18.5	81	0.6%	9
A-0.2-B-9-C-20	774.64	369	150	37.1	81	0.2%	9
A-0.2-B-12-C-30	774.64	369	150	55.7	81	0.2%	12
A-0.2-B-18-C-30	774.64	369	150	55.7	81	0.2%	18
A-0.2-B-9-C-30	774.64	369	150	55.7	81	0.2%	9
A-0-B-0-C-10	774.64	369	150	18.5	81	0	0
A-0-B-0-C-0	774.64	369	150	0	81	0	0

2.4. Preparation of Samples

Conventional ceramsite concrete was prepared in accordance with the technical Standard for Lightweight Aggregate Concrete Application (JGJ/T 12-2019). There are related definitions of ceramsite, that is, dry state, air-dry state, saturated surface dry state, and wet state. On the basis of research and trials, the best conditions for coarse aggregate were selected as dry ceramsite on a saturated surface. The dry state of a saturated surface refers to both the inside and outside of the ceramsite being saturated, with no clear water on the external surface. In this state, the ceramsite has little influence on the overall water-cement ratio during mixing. Rubber particles were sealed in advance [31] and were directly removed for use during the test. Basalt fibers were dried in advance to avoid moisture contamination and agglomeration [34]. In the process of mixing, the fibers were scattered into the mixing barrel in batches, and when the fibers were found to be bonded, they were manually separated before being put in, especially paying attention to the agglomeration of long fibers. After mixing, several working properties, including the slump, were measured, and the mold was installed at the same time. Rubber particles have high hydrophobicity and serious bleeding, so the molding process should be rapid [35].

3. Test Results and Discussion

3.1. Analysis of Compressive Strength

After specimen curing for 3 and 28 days, the compressive strength test was carried out. The test results showed that the compressive strength of the rubber ceramsite concrete

specimen improved significantly with the increase in the fiber content with the condition that the length of basalt fiber remained unchanged, as shown in Figure 1.

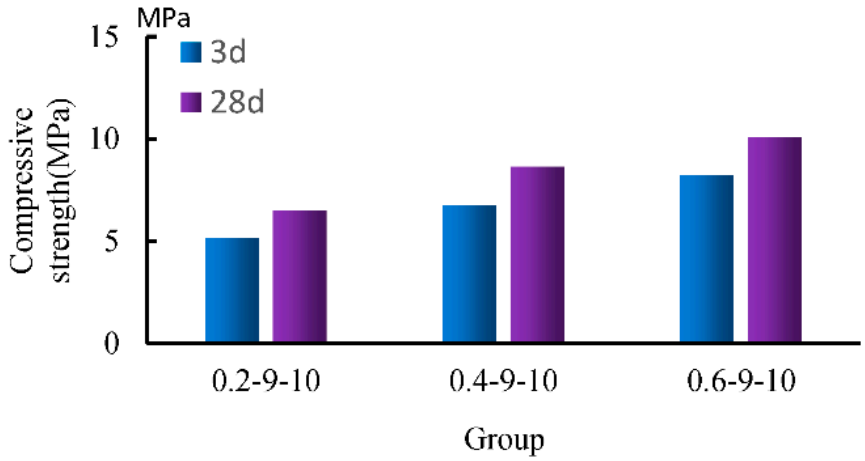

Figure 1. Diagram of compressive strength variation with fiber content.

The test results showed that there is little difference between the 9 mm length combination and the 18 mm length combination strength, but the 12 mm length combination showed obvious improvement. At 3-day strength, the compressive strength of the 12 mm combination increased by 19.9% compared with the 9 mm combination, and 23.7% compared with the 18 mm combination. This shows that the influence trend of basalt fiber length on compressive strength increases first and then decreases, and the use of an appropriate length improves compressive strength, as shown in Figure 2.

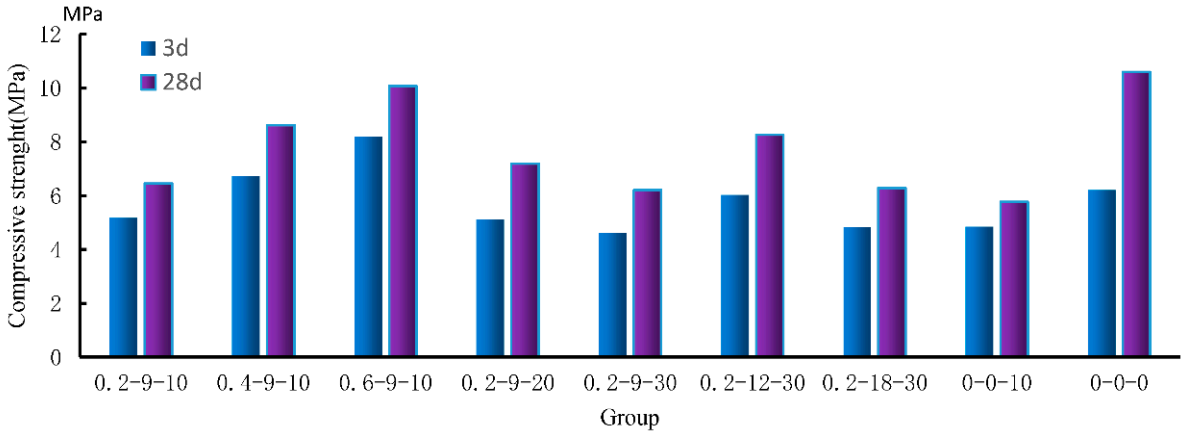

Figure 2. Diagram of multi-age compressive strength variation in each group.

Meanwhile, by comparing group A-0.2-B-9-C-10 and group A-0-B-0-C-10 in Figure 2, it can be concluded that basalt fiber has an improvement effect on the compressive strength of rubber ceramsite concrete, which increases by 6.2%. By comparative analysis of the A-0-B-0-C-10 group and A-0-B-0-C-0 group, we found that the addition of rubber does significantly weaken the compressive strength of ceramsite concrete. In the three-day strength test, the compressive strength of the control group, adding 10% rubber, was 21.9% lower than that of ordinary ceramsite concrete. This decrease gradually increased as the curing time went on and reached 45.5% at 28 days.

Figure 3 shows the influence of different rubber content on the compressive strength. The A-0.2-B-9-C-10 group, A-0.2-B-9-C-20 group, and A-0.2-B-9-C-30 group represent the compressive strength of three different rubber particle contents. We observed that the compressive strength of ceramsite concrete increased first and then decreased with the increase in the rubber content. An appropriate replacement rate could reduce the

compressive strength weakening caused by rubber incorporation, which is consistent with the research results of Karunarathna Sachinthani et al. [36–39].

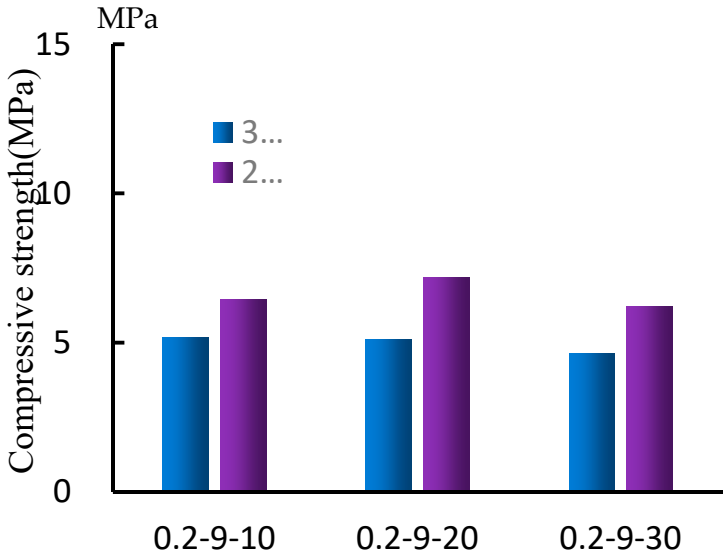

Figure 3. Compressive strength as a function of rubber content.

3.2. Analysis of Splitting Tensile Strength

Figure 4 shows the variation of the splitting tensile strength of rubber ceramsite concrete mixed with basalt fiber. It shows that the change of the length of basalt fiber has no significant influence on the improvement of the splitting tensile strength, but the increase in the content of basalt fiber contributes to an improvement of its strength. The addition of rubber greatly reduced the splitting tensile strength of the specimen. Compared with the A-0-B-0-C-10 group, the splitting tensile strength of the A-0-B-0-C-0 group decreased by 60.7%. However, the splitting tensile strength of the specimen did not show a corresponding change trend with the increase in the rubber content. Considering that there is no significant correlation between the splitting tensile strength and the internal porosity of the specimen, the relationship between the two needs to be demonstrated by further tests.

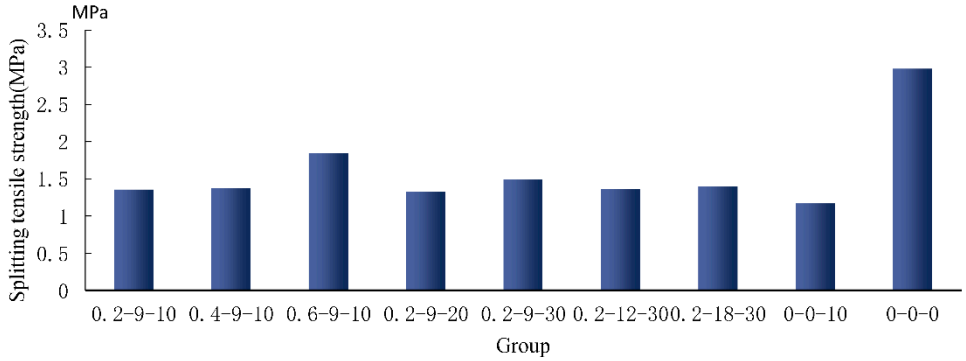

Figure 4. Diagram of variation of the splitting tensile strength.

3.3. Water Absorption Analysis

Three specimens were taken from each group for the water absorption test, and the average value was taken as the final water absorption. Figure 5 shows the final results of the water absorption test, and the overall curve shows a relatively obvious change rule. The content of basalt fiber in groups 1, 2, and 3 increased step by step, and the water absorption rate showed a linear decrease. The increase in the content of basalt fiber can effectively reduce the pores inside the specimen and reduce the water absorption rate. The rubber content of the 0.2-9-10, 0.2-9-20, and 0.2-9-30 combinations increased step by step,

and the water absorption rate was clearly observed to increase, indicating that the rubber incorporation would lead to the increase in porosity and increase the water absorption rate. The three groups of 0.2-9-30, 0.2-12-30, and 0.2-18-30 were the control groups of basalt fiber length. Compared with the combination of 9 and 18 mm, the combination of 12 mm length showed a better performance and the lowest water absorption rate, indicating that it had fewer internal pores, which was also consistent with the performance of 12 mm fiber length in terms of compressive strength. The comparison between groups 0.2-9-10 and 0-0-10 proved that the addition of basalt fiber can effectively reduce the formation of internal pores and water absorption of rubber ceramsite concrete. The comparison between the 0-0-0 group and the previous eight groups showed that the addition of rubber increases the generation of internal pores of the specimen and affects the performance of its compressive strength, which is similar to the findings of many researchers [40].

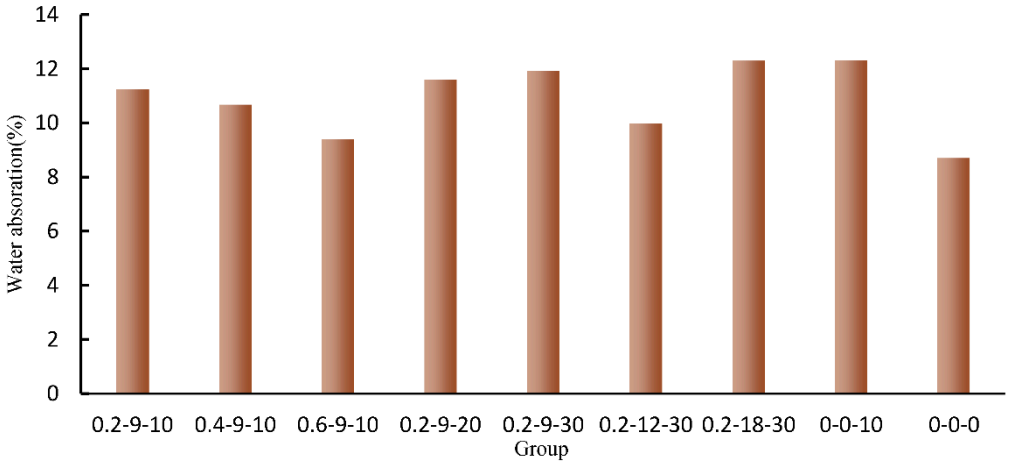

Figure 5. Curve of water absorption change.

Figure 6 shows the relationship between the change of water absorption and the change of compressive strength, and it can be observed that the two are significantly negatively correlated. This is because the increase or decrease in water absorption characterizes the number of pores inside the specimen. The internal compactness of the specimen is related to the compressive strength performance of the specimen, and a specimen with internal compactness has better compressive strength performance.

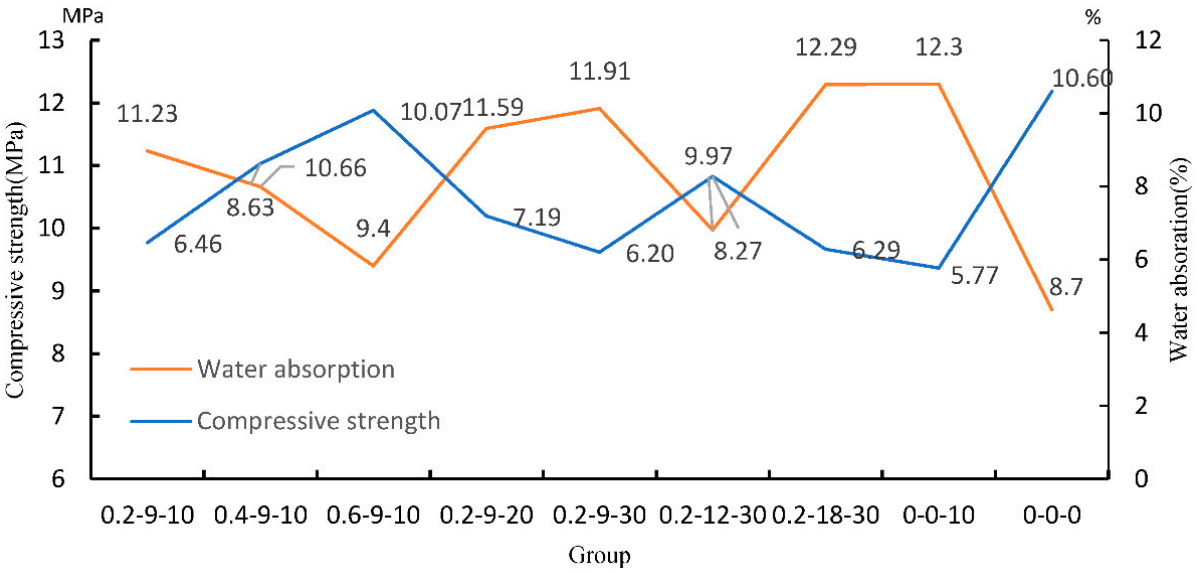

Figure 6. Diagram of water absorption and compressive strength.

3.4. SEM Analysis

An SEM was used to observe the internal microstructure of the specimens [41–43], verify the action law of basalt fiber and rubber particles, investigate the combination of the aggregate with the cement matrix, and observe the structural characteristics of the aggregate itself. The 50-fold microscopic image of rubber particles and ceramic particles is shown in Figure 7. It can be observed that the ceramic particles have typical porosity, and holes of various sizes are widely distributed. The rubber particles as a whole are long prisms with irregular outer edges, and the surface of the multi-crystalline material is considered to be free sulfur crystallization or vulcanizing agent, with the overflow of semi-vulcanized products forming crystallization. Figure 8 shows the 10-fold microscopic image of the rubber particles. It can be observed that the particle size distribution of the rubber particles is very different. The irregular shape and differential particle size distribution of the rubber particles are the important reasons that the compressive strength of 20% rubber particles is greater than that of 10% rubber particles. The filling effect of small rubber particles in the porous ceramic can help resist the invasion of water molecules, which is of great help to improve the mechanical properties.

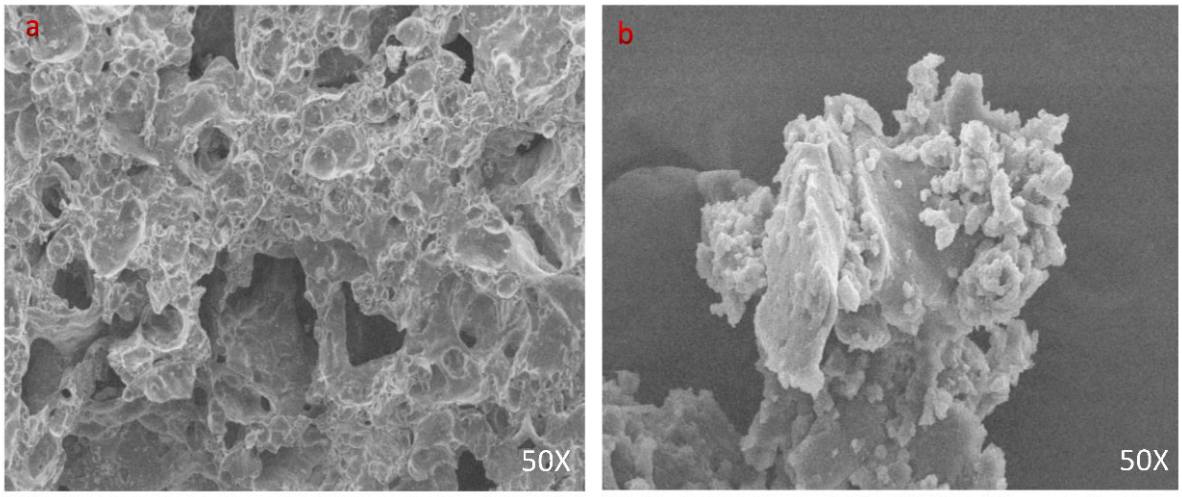

Figure 7. (**a**) Microscopic appearance of ceramsite; (**b**) microscopic appearance of rubber particles.

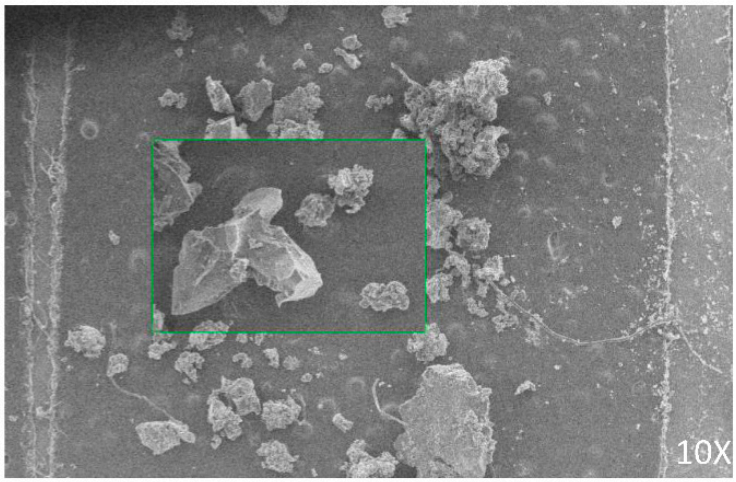

Figure 8. Microscopic appearance of rubber particles with multiple particle sizes.

Figures 9 and 10 are microscopic images of the interface between the basalt fibers and cement matrix. In Figure 9, 18 mm basalt fiber is agglutinated, which is an unfavorable phenomenon that is more likely to occur in the mixing process of longer fibers. The

agglutinated fibers cannot fully carry out their function, and at the same time, they have weak forces and are more likely to produce cracks. Figure 10 shows a microscopic image of the combination of 12 mm fiber length. It can be observed that the fiber is well dispersed and closely combined with the cement matrix, playing a good bridging role and optimizing the connection between the aggregate and matrix.

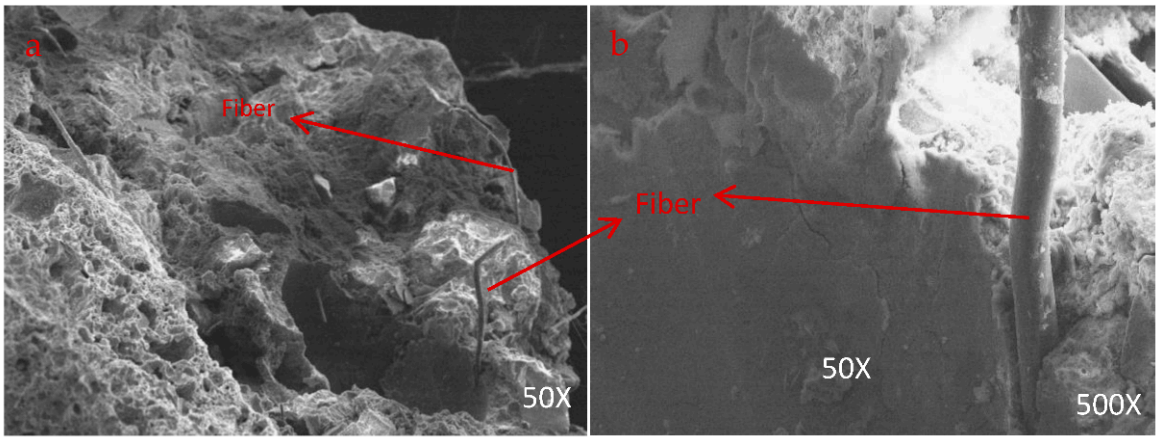

Figure 9. (**a**) Bonding interface of 12 mm basalt fiber and cement matrix at 50X; (**b**) Bonding interface of 12 mm basalt fiber and cement matrix at 500X.

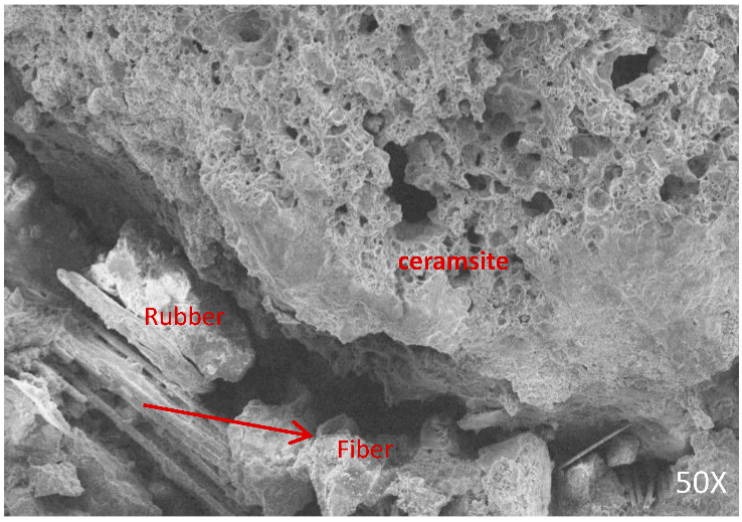

Figure 10. Microscopic diagram of rubber particles distributed in cracks.

Figure 10 shows the distribution of rubber aggregate in the cracks. It can be observed that rubber particles remained in the cracks between the substrates. At the same time, an obvious interfacial transition zone can be observed. There is a good combination between ceramsite and the cement matrix, without obvious cracks. In the process of crushing and soaking in anhydrous ethanol, ceramsite and rubber particles on the surface escaped and formed many pores and pits on the surface, as shown in Figure 11. At the same time, it can be observed in Figure 11 that potholes formed in the interface transition zone, which is different from the pothole characteristics of the round ceramsite. The potholes formed by rubber escape weakened the interface transition zone and adversely affected the compressive strength. Combined with Figure 10, rubber, as a crack filling material, can effectively serve as a slow-release medium of energy. Under continuous stress, the energy absorption capacity of rubber particles can help slow down the generation and expansion of cracks.

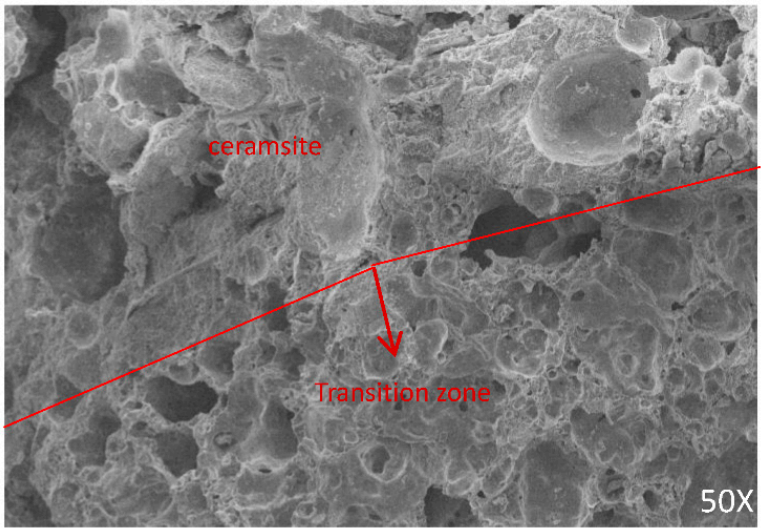

Figure 11. Micrograph of the porous surface of the cement matrix and ceramsite.

3.5. Ultrasonic Wave Velocity Test Analysis

An ultrasonic wave velocity test was used as an auxiliary means to evaluate the uniformity inside the specimen. The measured ultrasonic wave velocity can be used to characterize the number of pores and aggregate distribution in different parts of the specimen. The specimen was mainly composed of matrix, aggregate, and pores. The propagation velocity of ultrasonic waves is different, so it is feasible to use different ultrasonic wave velocities to characterize the internal structure. Figure 12 shows the variation of ultrasonic velocity for different groups.

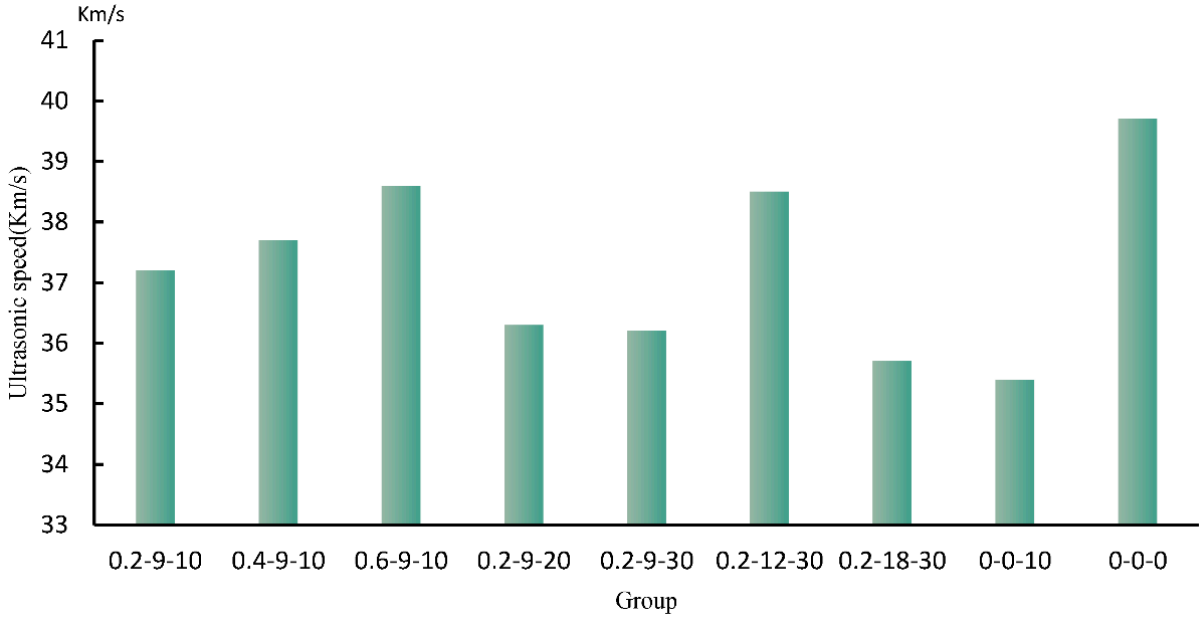

Figure 12. The diagram of the ultrasonic wave velocity.

Figures 13 and 14 compare the variation trend of the ultrasonic wave velocity, water absorption rate, and compressive strength. It can be observed that with the increase in the water absorption rate, the ultrasonic wave velocity gradually decreased, indicating that the internal cavity keeps increasing, and the compressive strength decreases.

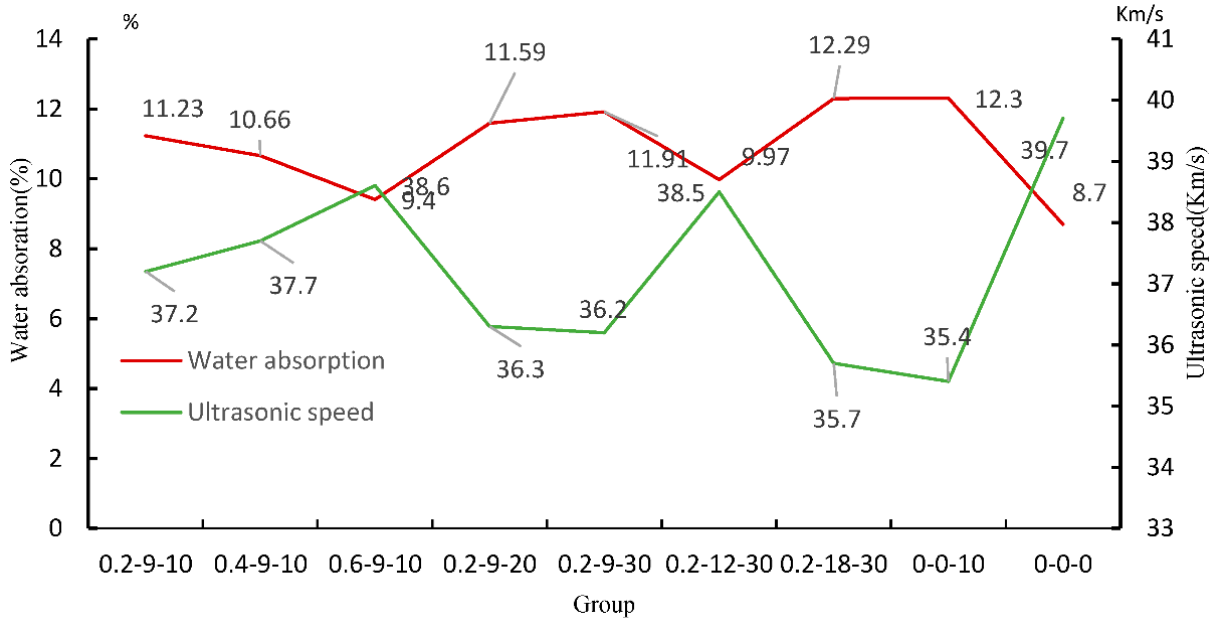

Figure 13. Contrast diagram of the ultrasonic wave velocity and water absorption.

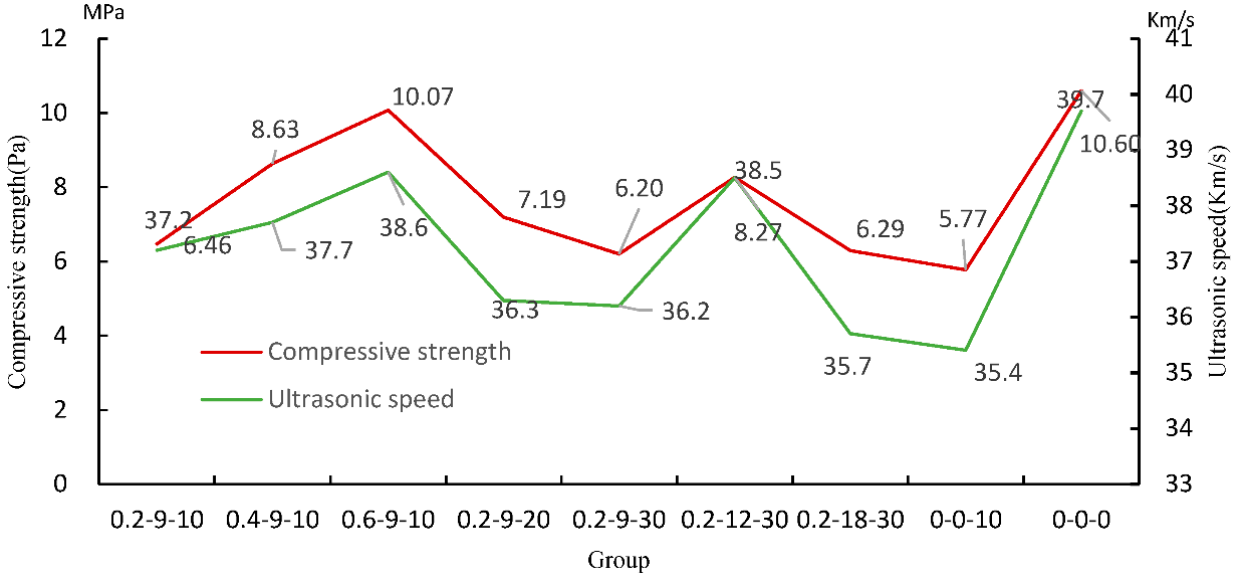

Figure 14. Contrast diagram of the ultrasonic wave velocity and compressive strength.

4. Conclusions

Basalt fiber modified rubber ceramsite concrete is an innovative solution based on engineering practices. After testing the mechanical properties of compressive strength and splitting tensile strength, as well as carrying out microscopic, ultrasonic, and water absorption tests, the following conclusions were reached:

(1) Basalt fiber can significantly improve the strength of rubber ceramsite concrete, and the improvement effect is the best when the dosage is 0.6%. When the basalt fiber length is 12 mm, the lifting effect is better. The splitting tensile strength of rubber ceramsite concrete recovered after adding basalt fiber, but the recovery degree was not affected by fiber content and length. The optimal combination was obtained by adding 0.6% 12 mm basalt fiber to the concrete with a 20% rubber replacement rate, which is the optimal solution based on multi-factor coupling conditions. Basalt fiber can play a structural role when concrete is under load, and the improvement of static mechanical properties is obvious.

(2) The compressive strength of concrete is negatively correlated with its water absorption. With the increase in water absorption, the internal porosity of concrete increases, and the compressive strength decreases accordingly. This is because an excessively high water absorption rate means that there are many cavities in the concrete, which become weak links and be the first to be destroyed when subjected to load.

(3) The irregular shape and large particle size range of rubber particles can be observed through the microscopic images of scanning electron microscopy. Filling in cracks can act as a channel for energy release and slow down the growth of cracks. Considering the specific change of water absorption between 10% rubber and 20% rubber, it is considered that the large holes on the ceramsite surface and the irregular shape of small rubber particles can complement each other and block a considerable part of the water molecule transport channels, thus reducing water absorption.

In conclusion, the addition of basalt fiber can effectively improve the mechanical property weakening of ceramsite concrete caused by the addition of rubber. At the same time, it is feasible to use water absorption to characterize the internal pores of the concrete and to use ultrasonic to evaluate the uniformity of the concrete. Choosing rubber particles with a proper particle size and dosage, and mixing basalt fiber with reasonable length and dosage, can help rubber ceramsite concrete recover strength and ensure its suitability for more engineering application scenarios.

Author Contributions: C.B. was mainly responsible for the ideas and the formulation or evolution of overarching research goals and aims. D.Z. was responsible for writing and for the first translation work. L.L. was mainly responsible for downloading and filing documents. He also researched and analyzed data in a variety of ways. X.L. was responsible for conducting the research and investigation process. Y.S. mainly reviewed the translation of the thesis and was responsible for the project administration. Z.Y. provided guidance on the test plan and provision of external test equipment. He was also responsible for solving the difficult problems during the experiment. L.Y. and Q.W. were fund providers, solving the problem of fund consumption in the process of paper writing. They also provided the ideas of original test. All authors have read and agreed to the published version of the manuscript.

Funding: This research was funded by the project of the Natural Science Foundation of Chongqing municipality (cstc2021jcyj-msxmX0444), as well as the project of Chongqing Construction science and Technology Plan (2021 No. 1–6) and the project of Chongqing Bureau of Human Resources and Social Security (cx2020008). This study was also supported by the open fund of Chongqing Key Laboratory of Energy Engineering Mechanics & Disaster Prevention and Reduction (EEMDPM2021103), the cooperation project of the Ministry of Education "Chunhui Planning" (Z2015147), the postgraduate science and technology innovation project in Chongqing University of Science and Technology (No. YKJCX2120601), and the fund of State Key Laboratory of Bridge Engineering Structural Dynamics, Key Laboratory of Bridge Earthquake Resistance Technology, Ministry of Communications, PRC.

Institutional Review Board Statement: Not applicable.

Informed Consent Statement: Not applicable.

Acknowledgments: Thanks to L.Y. for the guidance during the experiment; to Q.W. for the experimental materials and guidance; to all the teachers and classmates who worked hard during the experiment.

Conflicts of Interest: The authors declare that they have no known competing financial interests or personal relationships that could have appeared to influence the work reported in this paper.

References

1. Thomas, B.S.; Gupta, R.C. Long term behaviour of cement concrete containing discarded tire rubber. *J. Clean. Prod.* **2015**, *102*, 78–87. [CrossRef]
2. Amari, T.; Themelis, N.J.; Wernick, I.K. Resource recovery from used rubber tires. *Resour. Policy* **1999**, *25*, 179–188. [CrossRef]
3. Steyn, Z.C.; Babafemi, A.J.; Fataar, H.; Combrinck, R. Concrete containing waste recycled glass, plastic and rubber as sand replacement. *Constr. Build. Mater.* **2021**, *269*, 121242. [CrossRef]

4. Prasad, M.G.; Golla, S.Y.; Prabhanjan, N.; Krishna, A.S.; Alok, G. Mechanical properties of rubberized concrete using truck scrap rubber. *Mater. Today Proc.* **2021**, *39*, 849–854. [CrossRef]
5. Deredas, K.; Kępczak, N.; Urbaniak, M. Influence of doping with styrene-butadiene rubber on dynamic and mechanical properties of polymer concrete. *Compos. Struct.* **2021**, *268*, 113998. [CrossRef]
6. Zhang, S.C.; Geng, O.; Zhang, R.J. Experimental study on mechanical properties of waste tire rubber powder ceramsite concrete wallboard. *Ind. Constr.* **2016**, *46*, 93–97.
7. Gerges, N.N.; Issa, C.A.; Fawaz, S.A. Rubber concrete: Mechanical and dynamical properties. *Case Stud. Constr. Mater.* **2018**, *9*, e00184. [CrossRef]
8. Mhaya, A.M.; Huseien, G.F.; Faridmehr, I.; Abidin, A.R.Z.; Alyousef, R.; Ismail, M. Evaluating mechanical properties and impact resistance of modified concrete containing ground Blast Furnace slag and discarded rubber tire crumbs. *Constr. Build. Mater.* **2021**, *295*, 123603. [CrossRef]
9. Akçaoğlu, T.; Tokyay, M.; Çelik, T. Assessing the ITZ microcracking via scanning electron microscope and its effect on the failure behavior of concrete. *Cem. Concr. Res.* **2005**, *35*, 358–363. [CrossRef]
10. Wu, Y.F.; Kazmi, S.M.S.; Munir, M.J.; Zhou, Y.; Xing, F. Effect of compression casting method on the compressive strength, elastic modulus and microstructure of rubber concrete. *J. Clean. Prod.* **2020**, *264*, 121746. [CrossRef]
11. Assaggaf, R.A.; Ali, M.R.; Al-Dulaijan, S.U.; Maslehuddin, M. Properties of concrete with untreated and treated crumb rubber–A review. *J. Mater. Res. Technol.* **2021**, *11*, 1753–1798. [CrossRef]
12. He, L.; Ma, Y.; Liu, Q.; Mu, Y. Surface modification of crumb rubber and its influence on the mechanical properties of rubber-cement concrete. *Constr. Build. Mater.* **2016**, *120*, 403–407. [CrossRef]
13. Zhu, H.; Wang, Z.; Xu, J.; Han, Q. Microporous structures and compressive strength of high-performance rubber concrete with internal curing agent. *Constr. Build. Mater.* **2019**, *215*, 128–134. [CrossRef]
14. Si, R.; Guo, S.; Dai, Q. Durability performance of rubberized mortar and concrete with NaOH-Solution treated rubber particles. *Constr. Build. Mater.* **2017**, *153*, 496–505. [CrossRef]
15. Pham, T.M.; Elchalakani, M.; Hao, H.; Lai, J.; Ameduri, S.; Tran, T.M. Durability characteristics of lightweight rubberized concrete. *Constr. Build. Mater.* **2019**, *224*, 584–599. [CrossRef]
16. Youssf, O.; Hassanli, R.; Mills, J.E.; Skinner, W.; Ma, X.; Zhuge, Y.; Roychand, R.; Gravina, R. Influence of mixing procedures, rubber treatment, and fibre additives on rubcrete performance. *J. Compos. Sci.* **2019**, *3*, 41. [CrossRef]
17. Mohammadi, I.; Khabbaz, H.; Vessalas, K. In-depth assessment of Crumb Rubber Concrete (CRC) prepared by water-soaking treatment method for rigid pavements. *Constr. Build. Mater.* **2014**, *71*, 456–471. [CrossRef]
18. Ateeq, M.; Al-Shamma'a, A. Experimental study on the microwave processing of waste tyre rubber aggregates to enhance their surface properties for their use in rubberized bituminous mixtures. *Microw. Opt. Technol. Lett.* **2017**, *59*, 2951–2960. [CrossRef]
19. Ossola, G.; Wojcik, A. UV modification of tire rubber for use in cementitious composites. *Cem. Concr. Compos.* **2014**, *52*, 34–41. [CrossRef]
20. Herrera-Sosa, E.S.; Martínez-Barrera, G.; Barrera-Díaz, C.; Cruz-Zaragoza, E. Waste tire particles and gamma radiation as modifiers of the mechanical properties of concrete. *Adv. Mater. Sci. Eng.* **2014**, *2014*, 327856. [CrossRef]
21. Muhammad, B.; Ismail, M. Performance of natural rubber latex modified concrete in acidic and sulfated environments. *Constr. Build. Mater.* **2012**, *31*, 129–134. [CrossRef]
22. Ismail, M.; Muhammad, B.; Mohamad, N.A. Durability performance of natural rubber latex modified concrete. *Malays. J. Civ. Eng.* **2009**, *21*, 195–203.
23. Pereira, P.; Evangelista, L.; De Brito, J. The effect of superplasticizers on the mechanical performance of concrete made with fine recycled concrete aggregates. *Cem. Concr. Compos.* **2012**, *34*, 1044–1052. [CrossRef]
24. Takigawa, M.; Nemoto, H.; Hashimoto, S. Effectiveness of Thermal Stimulation of Superplasticizers on Fresh Properties of Cement Mortar. *Iran. J. Sci. Technol. Trans. Civ. Eng.* **2021**, 1–11. [CrossRef]
25. Dubey, R.; Kumar, P. Effect of superplasticizer dosages on compressive strength of self compacting concrete. *Int. J. Civ. Struct. Eng.* **2012**, *3*, 360–366.
26. Xu, J.; Kang, A.; Wu, Z.; Xiao, P.; Gong, Y. Effect of high-calcium basalt fiber on the workability, mechanical properties and microstructure of slag-fly ash geopolymer grouting material. *Constr. Build. Mater.* **2021**, *302*, 124089. [CrossRef]
27. Jabbar, A.M.; Hamood, M.J.; Mohammed, D.H. The effect of using basalt fibers compared to steel fibers on the shear behavior of ultra-high performance concrete T-beam. *Case Stud. Constr. Mater.* **2021**, *15*, e00702. [CrossRef]
28. Tayebi, M.; Nematzadeh, M. Post-fire flexural performance and microstructure of steel fiber-reinforced concrete with recycled nylon granules and zeolite substitution. *Structures* **2021**, *33*, 2301–2316. [CrossRef]
29. Altun, M.G.; Oltulu, M. Effect of different types of fiber utilization on mechanical properties of recycled aggregate concrete containing silica fume. *J. Green Build.* **2020**, *15*, 119–136. [CrossRef]
30. Manjunatha, M.; Seth, D.; Balaji, K.V.G.D.; Chilukoti, S. Influence of PVC waste powder and silica fume on strength and microstructure properties of concrete: An experimental study. *Case Stud. Constr. Mater.* **2021**, *15*, e00610.
31. Su, Z.J.; Guan, L.Y.; Shi, A.L. Working principle of environmental scanning electron microscope and its meteorological application. *Meteorol. Sci. Technol.* **2010**, *38*, 259–262.
32. Ridengaoqier, E.; Hatanaka, S.; Palamy, P.; Kurita, S. Experimental study on the porosity evaluation of pervious concrete by using ultrasonic wave testing on surfaces. *Constr. Build. Mater.* **2021**, *300*, 123959.

33. Chen, M.; Sun, Z.; Tu, W.; Yan, X.; Zhang, M. Behaviour of recycled tyre polymer fibre reinforced concrete at elevated temperatures. *Cem. Concr. Compos.* **2021**, *124*, 104257. [CrossRef]
34. Pham, T.M.; Lim, Y.Y.; Malekzadeh, M. Effect of pre-treatment methods of crumb rubber on strength, permeability and acid attack resistance of rubberised geopolymer concrete. *J. Build. Eng.* **2021**, *41*, 102448.
35. Habib, A.; Yildirim, U.; Eren, O. Mechanical and dynamic properties of high strength concrete with well graded coarse and fine tire rubber. *Constr. Build. Mater.* **2020**, *246*, 118502. [CrossRef]
36. Karunarathna, S.; Linforth, S.; Kashani, A.; Liu, X.; Ngo, T. Effect of recycled rubber aggregate size on fracture and other mechanical properties of structural concrete. *J. Clean. Prod.* **2021**, *314*, 128230. [CrossRef]
37. Ly, H.B.; Nguyen, T.A.; Tran, V.Q. Development of deep neural network model to predict the compressive strength of rubber concrete. *Constr. Build. Mater.* **2021**, *301*, 124081. [CrossRef]
38. Park, Y.; Abolmaali, A.; Kim, Y.H.; Ghahremannejad, M. Compressive strength of fly ash-based geopolymer concrete with crumb rubber partially replacing sand. *Constr. Build. Mater.* **2016**, *118*, 43–51. [CrossRef]
39. Hatungimana, D.; Yazici, Ş.; Orhan, Ş.; Mardani-Aghabaglou, A. Effect of styrene-butadiene copolymer (Sbr) latex on mechanical and transport properties of portland cement mortar. *J. Green Build.* **2020**, *15*, 185–197. [CrossRef]
40. Hatungimana, D.; Yazıcı, Ş.; Mardani-Aghabaglou, A. Effect of Polymer/Cement Ratio and Curing Regime on Polymer Modified Mortar Properties. *J. Green Build.* **2020**, *15*, 177–193. [CrossRef]
41. Jang, H.; So, S. Physical Properties and Environmental Performance of Steam-Cured Concrete Containing Flue-Gas Desulfurization Gypsum. *J. Green Build.* **2021**, *16*, 3–15. [CrossRef]
42. Mardani-Aghabaglou, A.; Felekoğlu, B.; Ramyar, K. The Role of Na_2O_{eq} Ratio on the Flowability and Strength Development of Cementitious Systems in the Presence of a Polycarboxylate Ether-Based Admixture. *J. Green Build.* **2019**, *14*, 93–110. [CrossRef]
43. Tuna Kayili, M.; Çelebi, G.; Guldas, A. Morphological, Mechanical, Thermal and Tribological Properties of Environmentally Friendly Construction Materials: Recycled LDPE Composites Filled by Blast Furnace Dust. *J. Green Build.* **2020**, *15*, 159–175. [CrossRef]